BANGMOD INTERNATIONAL JOURNAL OF MATHEMATICAL & COMPUTATIONAL SCIENCE
Volume 11 (2025)
Pages 135–156
ISSN: 2408-154X (Print)
ISSN: 3057-0557 (Online)
https://bangmodjmcs.com

Accessing the Thermodynamics of Ferromagnetic Sutterby Nanofluid with Effect of Homogeneous-Heterogeneous and Chemical Reactions

Auwalu Hamisu Usman[1,*], **Waris Khan**[2]

[1] *Department of Mathematical Sciences, Faculty of Physical Sciences, Bayero University, Kano, Nigeria*
E-mails: ahusman.mth@buk.edu.ng
[2] *Department of Mathematics and Statistics, Hazara University Mansehra, Khyber Pakhtunkhwa, Pakistan*
E-mails: wariskhan758@yahoo.com

**Corresponding author.*

Received: 31 October 2024 / Accepted: 30 April 2025

Abstract The work looked at how magnetic dipoles, pourosity parameters, and heat transfer affected the flow of ferromagnetic Sutterby nanofluid on a curved stretched sheet. The effects of gyrotactic microorganisms and homogeneous-heterogeneous reaction models are also considered. The momentum, energy, and gyrotactic microorganism equations, combined with the interaction of ferromagnetic particles, provide the governing equations for the problem, which are converted into ordinary differential equations using similarity transformations and solved using a strong homotopy analysis method (HAM). The impacts of parameters on dimensionless velocity, temperature, homogeneous-heterogeneous concentration, and motile microorganisms are graphically shown. The magnetic dipole effect and thermal radiation parameter increased the temperature. The homogeneous-heterogeneous concentration decreased as the homogeneous chemical reaction parameter increased, but the motile density of microorganisms decreased as the Lewis number increased. The results were consistent with numerous previously reported results, as predicted.

MSC: 80A20

Keywords: Cubic autocatalysis chemical reactions; curved surface; heat transfer; porous medium; ferromagnetic; Sutterby nanofluid

Published online: 26 May 2025

Published by Center of Excellence in Theoretical and Computational Science (TaCS-CoE)

Please cite this article as: A.H. Usman et al., Accessing the Thermodynamics of Ferromagnetic Sutterby Nanofluid with Effect of Homogeneous-Heterogeneous and Chemical Reactions, Bangmod Int. J. Math. & Comp. Sci., Vol. 11 (2025), 135–156. https://doi.org/10.58715/bangmodjmcs.2025.11.7

1. Introduction

The researchers' ongoing focus has been on non-Newtonian material flows. These materials are primarily used in biotechnology, geophysics, pharmaceutical, chemical, and nuclear industries, polymer solutions, cosmetics, oil storage, and paper production, among other things. In reality, not all non-Newtonian materials with behavioral shear patterns have a single constitutive relationship. A viscoelastic fluid is a non-Newtonian fluid with viscous and elastic deformation. Sutterby fluid is a good example of viscoelastic fluid and diluted polymer solutions [1, 2]. The Sutterby fluid model is specifically analogous to shear thickening and shear dilution in the case of high aqueous polymer solutions, such as methylcellulose, hydroxyethylcellulose, and carboxymethylcellulose [3]. Below is a list of references that contain studies on Sutterby fluids [4–6].
The flow of porous media attracts considerable interest among scientists, given their numerous kinds of real-world uses in the sector, including waste management, food storage, oil technologies, geothermal systems, packages, porous insulation, and waste extraction etc., the literature published a number of models that incorporate Darcy and Brinkman and Darcy Forchheimer. [7, 8]. Researchers are nowadays interested in studying porous media models. In the light of Darcy's law, the increase in pressure is directly linked to the average velocity of volume, and models developed on this concern. Viscous dissipation and thermophoresis analysis influences on the mixed convection Darcy-Forchheimer MHD in a fluid-saturated porous medium were reported by Kishan and Maripala [9]. In Darcy-Forchheimer porous space, Rauf et al. [10] studied the viscous fluid flow caused by thermal radiation over a curved moving surface. In nanofluid-saturated porous media, Jagadha and Amrutha [11] investigated the Darcy-Forchheimer mixed convection MHD boundary layer flow with viscous dissipation. More Sutterby fluid studies are included in the references [12–14].
Ferrofluids are a kind of magnetized fluid that are currently being studied and have an enormous influence on technology. Numerous industrial applications are widely used, including avionics, cooling agents, semiconductor processing, crystal processing, cooling, filtration, plastic drawing, lasers, robotics, fiber optics, and computer peripherals. Many scientists and researchers increased their ferrofluid study as a result of this. The study Andersson and Valnes [15] has looked into the visual effects of magnetic dipoles on ferrofluide. Hayat et al. [16] examined in the light of magnetic dipoles' role in the ferromagnetic Williamson fluid's radiative flow. some important studies on ferrofluid can be found in the references [17–19] .
Chemically reacting processes involving homogeneous-heterogeneous reactions have a wide range of practical and potential applications, including the hydrometallurgical industry, polymer production, ceramics, and biochemical systems, among others. Communication between homogeneous and heterogeneous reactions is extremely complicated, and the ability of these reactions to occur on and within the catalytic surface is extremely limited [20, 21]. For the study of homogeneous-heterogeneous response in viscous fluid flow over a flat surface a simple model was proposed by Merkin [22] which concluded that the surface reaction is influenced by the leading edge of the plate and that the homogeneous reaction is essential when the boundary layer developed. More recent work can be seen in [23–26].
Because of its indispensable uses in the polymer industry, engineering processes, and contemporary technologies, the curve surface flow is a widely discussed topic. Examples include melting and spinning, extruding polymers from dying materials, cooling large metal plates in a bath, or electrolytes; producing rubber and plastic sheets; drawing wire;

producing paper; thinning polymer sheets; winding rolls; glass fibers; liquid crystals during the condensation process; and so forth. The cooling and imprisonment procedures establish the ultimate amount of material. Sakiadis [27] was the first to present a flow study due to the curved moving surface. Recently, some reseacher presented important studies found in the references [28–30].

The practical application is that nanofluids are used to increase heat transfer in industrial cooling and heating applications such car engines, welding equipment, and high-heat-flow devices. They're also used in computer and power plant cooling systems.The present study concerned with the investigation on Darcy-Forchheimer of hydromagnetic Sutterby ferrofluid flow over the curve-stretching surface subject to homogeneousheterogeneous reactions model with the effect of magnetic dipole, viscous dissipation and porosity parameters which to best of my knowledge not considered in the literature. Through an appropriate process of similarity transformations, the equations are transformed into ordinary differential equations and obtained the solution by HAM [31–36]. However, many researchers like [37–40] solve their problems by HAM. The results obtained discussed graphically.

2. Formulation

The 2D incompressible ferromagnetic Sutterby nanofluid past a stretched curved sheet subject to homogeneousheterogeneous and chemical reactions is considered. However, the effect of viscous dissipation and magnetic dipole are taken into account. The curvilinear coordinates z and r are used. The surface (stretching) is curled in a radius circle R'. Considering the linear velocity $u = Az$ (c is constant), the sheet is stretched in and transverse to $z-$ direction and stretched $r-$ direction. The magnetic field strength is orthogonal to the flow direction (Fig. 1). The surface is soaked in a non-Darcy porous medium. The Reynolds number (magnetic) being smaller in the control problem, the setting ignored the induced magnetic and electrical field. However, heat Convection and mass transfer conditions are observed. Proposed by [41] form of a simple homogeneous-heterogeneous reaction model:

$$E_1 + 2E_2 \to 3E_2 \quad rate = k_c C_1 C_2^2. \tag{2.1}$$

With a single isothermal, on the catalytic surface first order reactions

$$E_1 + 2E_2 \to 3E_2 \quad rate = k_r C_1, \tag{2.2}$$

with C_1 and C_2 as the chemical species concentrations of E_1 and E_2 respectively, k_c and k_r are the rate constants. The nature of both reaction processes assumed to be isothermal. The equations govern the flow in dimensional form based on the assumptions [16, 22, 23, 28]

$$\frac{\partial\{(r+R')v\}}{\partial r} + R'\frac{\partial u}{\partial z} = 0, \tag{2.3}$$

$$\frac{u^2}{r+R'} = \frac{1}{\rho}\frac{\partial p}{\partial r}, \tag{2.4}$$

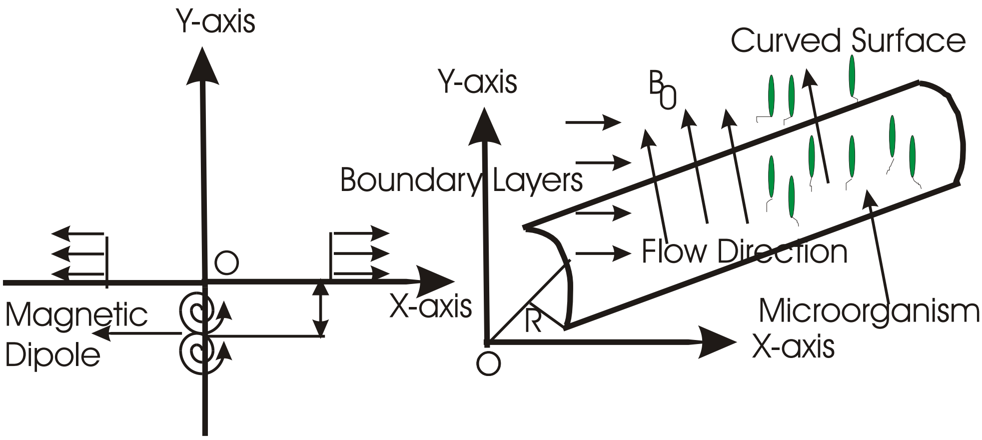

FIGURE 1. sketch picture of the problem.

$$
\begin{aligned}
&\rho\left(v\frac{\partial u}{\partial r}+\frac{R'u}{r+R'}\frac{\partial u}{\partial z}+\frac{uv}{r+R'}\right)=u_e\frac{du_e}{dz}+\frac{R'}{r+R'}\frac{\partial p}{\partial z}\\
&+\mu\left(\frac{\partial^2 u}{\partial r^2}-\frac{u}{(r+R')^2}+\frac{1}{r+R'}\frac{\partial u}{\partial r}\right)\\
&-k_0\left(\frac{2u}{(r+R')^2}\frac{\partial^3 u}{\partial z\partial r^2}+\frac{2v}{r+R'}\frac{\partial^3 u}{\partial r^3}+\frac{R'}{r+R'}\frac{\partial u}{\partial z}\frac{\partial^2 u}{\partial r^2}-\frac{2R'}{(r+R')^2}\frac{\partial u}{\partial r}\frac{\partial^2 u}{\partial r\partial z}\right)\\
&-\frac{\mu S_1}{k_o^*}u-\frac{\rho C_b S_1}{\sqrt{k_o^*}}u^2+\mu_o M\frac{\partial H}{\partial z},
\end{aligned}
\tag{2.5}
$$

$$
\begin{aligned}
&(\rho C_p)\left(\frac{R'u}{r+R'}\frac{\partial T}{\partial z}+v\frac{\partial T}{\partial r}\right)=\frac{k_T}{r+R'}\left[\frac{\partial T}{\partial r}+(r+R')\frac{\partial^2 T}{\partial r^2}\right]\\
&+\left(u\frac{\partial H}{\partial z}+v\frac{\partial H}{\partial r}\right)\mu_o T\frac{\partial M}{\partial T}-\frac{k_T}{r+R'}\left(\frac{\partial q_r}{\partial r}(r+R')\right),
\end{aligned}
\tag{2.6}
$$

$$
\frac{R'}{r+R'}u\frac{\partial C_1}{\partial z}+v\frac{\partial C_1}{\partial r}=D_{E_1}\frac{\partial^2 C_1}{\partial r^2}-k_c C_1 C_2,
\tag{2.7}
$$

$$
\frac{R'}{r+R'}u\frac{\partial C_2}{\partial z}+v\frac{\partial C_2}{\partial r}=D_{E_2}\frac{\partial^2 C_2}{\partial r^2}+k_c C_1 C_2,
\tag{2.8}
$$

$$
\left(\frac{R'}{r+R'}\right)u\frac{\partial N}{\partial z}+v\frac{\partial N}{\partial r}+\frac{bW_c}{C_w-C_\infty}\frac{\partial\left(N\frac{\partial C}{\partial r}\right)}{\partial r}=D_m\frac{\partial^2 N}{\partial r^2},
\tag{2.9}
$$

with boundary conditions

$$u = Az = U_w(z), \;\; v = 0, \; -K\frac{\partial T}{\partial r} = h_1\big(T_w - T\big), \; D_{E_1}\frac{\partial C_1}{\partial r} = k_r C_1,$$

$$D_{E_2}\frac{\partial C_2}{\partial r} = -k_r C_1, \;\; N = N_w \;\; at \;\;\; r = 0,$$

$$u \to u_e = 0, \quad \frac{\partial u}{\partial r} \to 0, \quad v \to 0, \quad T \to T_\infty, \;\; C_1 \to C_0, \;\; C_2 \to 0, \tag{2.10}$$

$$N \to N_\infty \quad as \quad r \to \infty, \tag{2.11}$$

where components velocity are (u,v) in the $z-$ direction(radial) and $r-$ direction(transverse), diffusion coefficient D_{E_1} and D_{E_2}, k_0 is the short memory coefficient, fluid thermal conductivity k_T, fluid density ρ, dynamic viscosity μ, fluid electrical conductivity σ, fluid heat capacitance (ρc_p), b chemotaxis, S_1 porosity of porous medium, first order chemical reaction parameter K_c, magnetic permeability μ_o, gyrotactic Speed cell W_c, Microorganism diffusion D_m, T the temperature, N the gyrotactic Microorganism and T_∞, and N_∞ stand for the temperature, and Density of microorganisms at infinity respectively.

2.1. Magnetic Dipole

The magnetic scalar potential Φ can identify magnetic dipole effects shown in eq. (2.12). Because of the magnetic dipole, the properties of the magnetic field affect the flow of ferrofluid.

$$\Phi = \frac{\gamma}{2\pi}\frac{z}{z^2 + (r+c)^2} \tag{2.12}$$

at the source, magnetic field strength represent by γ. With H_z and H_r taking as the components of magnetic field shown in Eqs. (2.13) and (2.14).

$$H_z = -\frac{\partial \Phi}{\partial z} = \frac{\gamma}{2\pi}\frac{z^2 - (r+c)^2}{[z^2 + (r+c)^2]^2}, \tag{2.13}$$

$$H_r = -\frac{\partial \Phi}{\partial r} = \frac{\gamma}{2\pi}\frac{2z(r+c)}{[z^2 + (r+c)^2]^2}. \tag{2.14}$$

The magnetic body strength is stated at (2.15) because it is typically proportional to the elements of the magnetic field gradient.

$$H = \sqrt{H_z^2 + H_r^2}. \tag{2.15}$$

The approximate linear form of magnetization M by temperature T given in eq. (2.16)

$$M = K_1(T - T_\infty). \tag{2.16}$$

A ferromagnetic coefficient is identified by the value of K_1, see Figure 1.
Using the transformations [10] below

$$u = Azf'(\zeta), \;\; v = -\left(\frac{R'}{r+R'}\right)\sqrt{A\nu}f(\zeta), \;\; p = \rho A^2 z^2 p(\zeta), \;\; \zeta = r\sqrt{\frac{A}{\nu}},$$

$$\theta(\zeta) = \frac{T - T_\infty}{T_w - T_\infty}, \;\; C_1 = c_0\phi_1(\zeta), \;\; C_1 = c_0\phi_1(\zeta), \;\; \chi(\zeta) = \frac{N - N_\infty}{N_w - N_\infty}. \tag{2.17}$$

$$p' = \frac{f'^2}{\zeta + \alpha_1}, \tag{2.18}$$

$$
\begin{aligned}
& f''' + \frac{1}{\zeta+\alpha_1} f'' - \frac{1}{(\zeta+\alpha_1)^2} f' + \left(\frac{\alpha_1}{\zeta+\alpha_1}\right)\left[f f'' - f'^2 + \frac{1}{\alpha_1} f' f \right] \\
& - \alpha \left[\frac{(2+\alpha_1)}{(\zeta+\alpha_1)^2} f' f''' - \frac{2\alpha_1}{(\zeta+\alpha_1)^2} (f f'''' - f''^2) \right] - P_1 f' - L_i f'^2 \\
& + \frac{2\beta}{(\zeta+d)^4} \theta + 2\left(\frac{\alpha_1}{\zeta+\alpha_1}\right) p = 0, \qquad (2.19)
\end{aligned}
$$

$$
\begin{aligned}
& (1+Rd)\left(\theta'' + \frac{\theta'}{(\zeta+\alpha_1)}\right) + Pr\left(\frac{\alpha_1}{\zeta+\alpha_1}\right) f\theta' + \frac{2\beta\lambda(\theta-\epsilon) f}{(\zeta+d)^3} \\
& + \beta\lambda(\theta-\epsilon)\left[\frac{2f'}{(\zeta+d)^4} + \frac{4f}{(\zeta+d)^5}\right] = 0, \qquad (2.20)
\end{aligned}
$$

$$
\phi_1'' + Sc\frac{\alpha_1}{(\zeta+\alpha_1)} f\phi_1' - ScK_c\phi_1\phi_2^2 = 0, \qquad (2.21)
$$

$$
\delta\phi_2'' + Sc\frac{\alpha_1}{(\zeta+\alpha_1)} f\phi_2' - ScK_c\phi_1\phi_2^2 = 0, \qquad (2.22)
$$

$$
\chi'' + Pe\left[\phi'\chi' + \phi''\chi + N_\delta\phi''\right] + Le\left(\frac{\alpha_1}{\zeta+\alpha_1}\right) f\chi' = 0. \qquad (2.23)
$$

When the pressure term is removed from integrate (2.18) in order to obtain p and substitute it, (2.19) becomes

$$
\begin{aligned}
& f''' + \frac{1}{\zeta+\alpha_1} f'' - \frac{1}{(\zeta+\alpha_1)^2} f' + \left(\frac{\alpha_1}{\zeta+\alpha_1}\right)\left[f f'' - f'^2 + \frac{1}{\alpha_1} f' f \right] + De f'' f''' \\
& - P_1 f' - L_i f'^2 + \frac{2\beta}{(\zeta+d)^4}\theta + \left(\frac{\alpha_1}{(\zeta+\alpha_1)^2}\right)(2 f f'' - f'^2) = 0, \qquad (2.24)
\end{aligned}
$$

given the boundary conditions below

$$
\begin{aligned}
& f'(0) = 1, f(0) = 0, f(\infty) = 0, f''(\infty) = 0, && (2.25) \\
& \theta'(0) = -B_{i1}[1-\theta(0)], \theta(\infty) = 0, && (2.26) \\
& \phi_1'(0) = k_r\phi_1(0), \phi_2'(0) = -k_r\phi_1(0), \phi_1(\infty) = 1, \phi_2(\infty) = 0, && (2.27) \\
& \chi'(0) = 1, \chi(\infty) = 0. && (2.28)
\end{aligned}
$$

The assumption that the diffusion coefficients D_{E_1} and D_{E_2} are equivalent arises from the expectation in many applications that the diffusion coefficients E_1 and E_2 of the chemical species will be of similar sizes. Using the assumption that $\delta = 1$, the Chaudhar and Merkin notion is applied [41] to produce the following equation

$$
\phi_1(\zeta) + \phi_2(\zeta) = 1. \qquad (2.29)
$$

Hence equations (2.21) and (2.22) finally becomes

$$
\phi_1'' + Scf\phi_1' - K_c\phi_1(1-\phi_1)^2 = 0, \qquad (2.30)
$$

with boundary equation as

$$
\phi_1'(0) = K_r\phi_1(0), \phi_1(\infty) = 1, \qquad (2.31)
$$

where α_1 curvature parameter, d dimensionless distance, α is the viscoelastic parameter, heat dissipation parameter λ, β the ferrohydrodynamic interaction, ε the curie temperature, Prandtl number Pr, radiation parameter Rd, the ratio of the diffusion coefficients is δ, De is Deborah number, the Schmidt number Sc, porosity parameter p_1, local inertia parameter is Li, K_c is the strength of the homogeneous reaction measure, K_r is the strength of heterogeneous reaction measure, Pe is Peclet number, Lewis number Le and thermal Biot number B_{i1} quantities are given by

$$\begin{aligned}
&\alpha_1 = R'\sqrt{\frac{A}{\nu}}, p_1 = \frac{\mu S_1}{\rho A k_o^*}, \alpha = \frac{k_0 A}{\rho\nu}, L_i = \frac{C_b S_1}{\sqrt{k_o^*}},\\
&\beta = \frac{\gamma\mu_o K_1 \rho(T_w - T_\infty)}{2\pi\mu^2}, Pr = \frac{\mu C_p}{k_T}, Le = \frac{\nu}{D_n}, \lambda = \frac{A\mu^2}{\rho(T_w - T_\infty)k_T},\\
&d = \sqrt{\frac{Ac^2}{\nu}}, De = \frac{mE^2(Az)^2}{\nu}, Rd = \frac{16\sigma^* T_\infty^3}{3kk^*},\\
&Sc = \frac{\nu}{D_{E_1}}, Pe = \frac{bW_c}{D_n}, N_\delta = \frac{N_\infty}{N_w - N_\infty}, B_{i1} = \frac{h_1}{k_T}\sqrt{\frac{\nu}{A}},\\
&K_r = k_r Re^{-\frac{1}{2}}/D_{E_1}, K_c = \frac{k_c c_0^2}{A}, Re = \frac{A}{\nu}, \epsilon = \frac{T_\infty}{T_\infty - T_w}.
\end{aligned} \tag{2.32}$$

In accordance with this, the intriguing physical quantities such as skin friction, local Nusselt, Sherwood, and density numbers are calculated below

$$\begin{aligned}
&C_f = \frac{\tau_{rz}}{\rho(Az)^2},\ Nu_z = \frac{-zq_w}{k_T(T_w - T_\infty)},\ Sh_z = \frac{-zq_m}{D(C_w - C_\infty)}\\
&Sn_z = \frac{-zq_n}{D_m(N_w - N_\infty)}
\end{aligned} \tag{2.33}$$

$$\begin{aligned}
&\tau_{rz} = \left(\mu u_r - \frac{k_0}{\rho}(uu_{zr} - 2u_r u_z)\right)|_{r=0},\ q_w = -k^*(T_r - q_r)|_{r=0},\\
&q_m = -DC_r|_{r=0}\ q_n = D_m N_r|_{r=0}
\end{aligned} \tag{2.34}$$

$$\begin{aligned}
&C_f = \frac{2}{Re_x^{0.5}} f''(0)\left(1 + \alpha f'(0)\right),\ Nu = -Re_x^{0.5}(1 + Rd)\theta'(0),\\
&Sn = -Re_x^{0.5}\chi'(0)
\end{aligned} \tag{2.35}$$

3. HAM Solutions methodology

The following are some of the benefits of using the Homotopy Analysis Method (HAM) to solve nonlinear equations: flexibility, convergence and independence. The steps are as follows: Taking the initial guesses and the linear operators as

$$f_0(\zeta) = (1 - e^{-\zeta}),\ \theta_0(\zeta) + \frac{B_{i1}}{1 + B_{i1}}e^{-\zeta},\ \phi_0(\zeta) + e^{-\zeta},\ \chi_0 = e^{-\zeta}. \tag{3.1}$$

the properties below satisfied by equation (3.1)

$$\begin{aligned}
&L_f(Q_1 + Q_2 e^{\zeta} + Q_3 e^{-\zeta}) = 0,\ L_\theta(Q_4 e^{\zeta} + Q_5 e^{-\zeta}) = 0,\\
&L_\phi(Q_6 e^{\zeta} + Q_7 e^{-\zeta}) = 0,\ L_\chi(Q_8 e^{\zeta} + Q_9 e^{-\zeta}) = 0,
\end{aligned} \tag{3.2}$$

with $Q_i(i = 1, ..., 9,)$ are arbitrary constants.
The problem's related zero order form is

$$\begin{aligned}
&(1-q)L_0[f(\zeta;q) - f_0(\zeta)] = qh_f N_f[f(\zeta,q), \theta(\zeta,q)],\\
&(1-q)L_0[\theta(\zeta;q) - \theta_0(\zeta)] = qh_f N_f[\theta(\zeta,q), f(\zeta,q)],\\
&(1-q)L_0[\phi_(\zeta,q) - \phi_0(\zeta)] = qh_f N_f[\phi_1(\zeta,q), f(\zeta,q)],\\
&(1-q)L_0[\chi(\zeta,q) - \chi_0(\zeta)] = qh_f N_f[\chi(\zeta,q), \phi_1(\zeta,q), f(\zeta,q)],
\end{aligned} \tag{3.3}$$

$$\begin{aligned}
&f(0,q) = 0, f'(0,q) = 1,\ f'(\infty,q) = A,\ \theta'(0,q) = -B_{i1}(1-\theta(0,q)),\\
&\theta(\infty,q) = 0, \phi_1'(0,q) = K_r\phi_1(0,q), \phi_1(\infty,q) = 0\ \chi'(0,q) = 1,\ \chi(\infty;q) = 0
\end{aligned} \tag{3.4}$$

$$\begin{aligned}
\mathbf{N}_f[f(\zeta,q), \theta(\zeta,q)] &= \frac{\partial^3 f(\zeta,q)}{\partial\zeta^3} + \frac{1}{\zeta+\alpha_1}\frac{\partial^2 f(\zeta,q)}{\partial\zeta^2} - \frac{1}{(\zeta+\alpha_1)^2}\frac{\partial f(\zeta,q)}{\partial\zeta}\\
&+ \left(\frac{\alpha_1}{\zeta+\alpha_1}\right)\left[f(\zeta,q)\frac{\partial^2 f(\zeta,q)}{\partial\zeta^2} - \left(\frac{\partial f(\zeta,q)}{\partial\zeta}\right)^2 + \frac{1}{\alpha_1}\frac{\partial f(\zeta,q)}{\partial\zeta}f(\zeta,q)\right]\\
&+ De\frac{\partial^2 f(\zeta,q)}{\partial\zeta^2}\frac{\partial^3 f(\zeta,q)}{\partial\zeta^3} - P_1\frac{\partial f(\zeta,q)}{\partial\zeta} - L_i\left(\frac{\partial f(\zeta,q)}{\partial\zeta}\right)^2\\
&+ \frac{2\beta}{(\zeta+d)^4}\theta(\zeta,q) + \left(\frac{\alpha_1}{(\zeta+\alpha_1)^2}\right)\left(2f(\zeta,q)\frac{\partial^2 f(\zeta,q)}{\partial\zeta^2} - \left(\frac{\partial f(\zeta,q)}{\partial\zeta}\right)^2\right),
\end{aligned} \tag{3.5}$$

$$\begin{aligned}
\mathbf{N}_\theta[\theta(\zeta,q), f(\zeta,q)] &= (1+Rd)\left(\frac{\partial^2\theta(\zeta,q)}{\partial\zeta^2} + \frac{1}{(\zeta+\alpha_1)}\frac{\partial\theta(\zeta,q)}{\partial\zeta}\right)\\
&+ Pr\left(\frac{\alpha_1}{\zeta+\alpha_1}\right)f(\zeta,q)\frac{\theta(\zeta,q)}{\partial\zeta} + \frac{2\beta\lambda(\theta(\zeta,q)-\epsilon)f(\zeta,q)}{(\zeta+d)^3}\\
&+ \beta\lambda(\theta(\zeta,q)-\epsilon)\left[\frac{2}{(\zeta+d)^4}\frac{\partial f(\zeta,q)}{\partial\zeta} + \frac{4f(\zeta,q)}{(\zeta+d)^5}\right],
\end{aligned} \tag{3.6}$$

$$\mathbf{N}_{\phi_1}[\phi_1(\zeta,q), f(\zeta,q)] = \frac{\partial^2\phi(\zeta,q)}{\partial\zeta^2} + Scf(\zeta,q)\frac{\partial\phi_1(\zeta,q)}{\partial\zeta} - K_c\phi_1(\zeta,q)(1-\phi_1(\zeta,q))^2, \tag{3.7}$$

$$\begin{aligned}
\mathbf{N}_\chi[\chi(\zeta,q)] &= \frac{\partial^2\chi(\zeta,q)}{\partial\zeta^2} + Pe\left[\frac{\partial\phi(\zeta,q)}{\partial\zeta}\frac{\partial\chi(\zeta,q)}{\partial\zeta} + \frac{\partial^2\phi_1(\zeta,q)}{\partial\zeta^2}\chi(\zeta,q) + N_\delta\frac{\partial^2\phi_1(\zeta,q)}{\partial\zeta^2}\right]\\
&+ Le\left(\frac{\alpha_1}{\zeta+\alpha_1}\right)f(\zeta,q)\frac{\partial\phi_1(\zeta,q)}{\partial\zeta},
\end{aligned} \tag{3.8}$$

where $q \in [0,1]$ be the embedding parameter and $\mathbf{N}_f$, $\mathbf{N}_\theta$, $\mathbf{N}_{\phi_1}$ and $\mathbf{N}_\chi$ are operators (nonlinear).
The m order problems deformation

$$L_f[f_m(\zeta,q) - \eta_m f_{m-1}(\zeta)] = h_f\mathcal{R}_{f,m}(\zeta), \tag{3.9}$$

$$L_\theta[\theta_m(\zeta,q) - \eta_m\theta_{m-1}(\zeta)] = h_\theta\mathcal{R}_{\theta,m}(\zeta), \tag{3.10}$$

$$\mathcal{L}_{\phi_1}[\phi_m(\zeta,q)-\eta_m\phi_{m-1}(\zeta)]=h_{\phi_1}\mathcal{R}_{\phi,m}(\zeta), \tag{3.11}$$

$$L_\chi[\chi_m(\zeta,q)-\eta_m\chi_{m-1}(\zeta)]=h_\chi\mathcal{R}_{\chi,m}(\zeta), \tag{3.12}$$

$$\begin{aligned}
&f_m(0)=f'_m(0)=f'_m(\infty)=0,\\
&\theta'_m(0)-B_{i1}\theta_m(0)=\theta_m(\infty)=0,\\
&\phi'_{1m}(0)=K_r\phi_{1m}(0),\phi_{1m}(\infty)=0,\\
&\chi'_m(0)=\chi_m(0)=\chi_m(\infty)=0,
\end{aligned} \tag{3.13}$$

$$\eta_m=\begin{cases}0, & \text{if } m\le 1,\\ 1, & \text{if } m>1,\end{cases} \tag{3.14}$$

$$\begin{aligned}
\mathcal{R}_f^m(\zeta)&=f'''_{m-1}+\frac{1}{\zeta+\alpha_1}f''_{m-1}-\frac{1}{(\zeta+\alpha_1)^2}f'_{m-1}\\
&+\left(\frac{\alpha_1}{\zeta+\alpha_1}\right)\left[\sum_{r=0}^{m-1}f_{m-1-r}f''_r-\left(\sum_{r=0}^{m-1}f'_{m-1-r}f'_r\right)^2+\frac{1}{\alpha_1}\sum_{r=0}^{m-1}f_{m-1-r}f'_r\right]\\
&+De\sum_{r=0}^{m-1}f''_{m-1-r}f'''_r-P_1f'_{m-1}-L_i\left(\sum_{r=0}^{m-1}f'_{m-1-r}f'_r\right)^2+\frac{2\beta}{(\zeta+d)^4}\theta_{m-1}\\
&+\left(\frac{\alpha_1}{(\zeta+\alpha_1)^2}\right)\left(2\sum_{r=0}^{m-1}f_{m-1-r}f''_r-\left(\sum_{r=0}^{m-1}f'_{m-1-r}f'_r\right)^2\right),
\end{aligned} \tag{3.15}$$

$$\begin{aligned}
\mathcal{R}_\theta^m(\zeta)&=\big(1+Rd\big)\left(\theta''_{m-1}+\frac{\theta'_{m-1}}{(\zeta+\alpha_1)}\right)+Pr\left(\frac{\alpha_1}{\zeta+\alpha_1}\right)\sum_{r=0}^{m-1}f_{m-1-r}\theta'_r\\
&\frac{2\beta\lambda(\theta_{m-1}-\epsilon)f_{m-1}}{(\zeta+d)^3}+\beta\lambda(\theta_{m-1}-\epsilon)\left[\frac{2f'_{m-1}}{(\zeta+d)^4}+\frac{4f_{m-1}}{(\zeta+d)^5}\right],
\end{aligned} \tag{3.16}$$

$$\mathcal{R}_{\phi_1}^m(\zeta)=\phi''_{1(m-1)}+\frac{\phi'_{1(m-1)}}{(\zeta+\alpha_1)}+\left(\frac{\alpha_1}{\zeta+\alpha_1}\right)Sc\sum_{r=0}^{m-1}f_{m-1-r}\phi'_r-\delta Sc\phi_{1(m-1)}, \tag{3.17}$$

$$\begin{aligned}
\mathcal{R}_\chi^m(\zeta)&=\chi''_{m-1}+Pe\left[\sum_{r=0}^{m-1}\phi'_{(1m-1-r)}\chi'_r+\sum_{r=0}^{m-1}\phi''_{1(m-1-r)}\chi_r+N_\delta\phi''_{1(m-1)}\right]\\
&+Le\left(\frac{\alpha_1}{\zeta+\alpha_1}\right)\sum_{r=0}^{m-1}f_{m-1-r}\chi'_r.
\end{aligned} \tag{3.18}$$

By solving the m order the general solutions are given by

$$f_m(\zeta) = f_m^*(\zeta) + Q_1 + Q_2 e^{\zeta} + Q_3 e^{-\zeta}, \tag{3.19}$$

$$\theta_m(\zeta) = \theta_m^*(\zeta) + Q_4 e^{\zeta} + Q_5 e^{-\zeta}, \tag{3.20}$$

$$\phi_{1m}(\zeta) = \phi_{1m}^*(\zeta) + Q_6 e^{\zeta} + Q_7 e^{-\zeta}, \tag{3.21}$$

$$\chi_m(\zeta) = \chi_m^*(\zeta) + Q_8 e^{\zeta} + Q_9 e^{-\zeta}, \tag{3.22}$$

where $(f_m^*(\zeta), \theta_m^*(\zeta), \phi_{1m}^*(\zeta), \chi_m^*(\zeta))$ are special solutions.

4. Results and Discussion

Figure 2 is used to investigate the impact of α_1 on the velocity profile. The figure shows how the fluid's velocity rises when the parameter α_1 increases. The efficiency of the ferromagnetic hydrodynamic interaction parameter β in the velocity profile is examined in Figure 3. In this case, the parameter β increase make the velocity to the decreasing behavior. In general, when β grows and the velocity falls, the resistance force classed as the Lorentz force increases. The Deborah number De on velocity function, which sheds light on the viscoelasticity properties of the Sutterby nanomaterial, is depicted in Figure 4. In this case, an increase in De causes Sutterby's flow velocity to increase. Fluid velocity increases when the hydrodynamic boundary layer thickness increases due to faster nanofluid motions. Figure 5 provides an explanation the characteristics of the porosity parameter $p1$. Because of the current porous medium's ability to slow down the field of flow, there is an increase in shear stress on the curved surface. This causes the velocity profile to trend downward and increases $p1$ values.

An analysis of the impact of $\alpha 1$ on the velocity profile is presented in Figure 6. The velocity component improves with a greater value of $\alpha 1$, as the image illustrates. Utilizing Figure 7, the influence of β on temperature is investigated. Here, the temperature rises as the β value rises. The parameter ε on the temperature properties are displayed in Figure 8. In the bigger value of ε, the temperature drops. Greater ε corresponds to increased fluid thermal conductivity, the temperature rises as a result of the additional heat being transferred from the surface into the liquid.The impact of the parameter λ on temperature is depicted in Figure 9. At this point the value of λ increases as the temperature drops. The temperature is physically lowered in the greater value of λ by the fluid's thermal conductivity. The effect of the $Bi1$ on temperature profile is displayed in Figure 10. It is observed that $Bi1$ value indicates an increase in temperature. In other words, $Bi1$ is directly proportional to the coefficient of heat transfer, which is larger value for $Bi1$, and depends on it. Temperature changes with rising Prandtl number Pr are shown in Figure 11. As the parameter Pr increases, the Sutterby nanofluid's temperature drops. Thermal diffusivity is referred to by the Prandtl number in physics. The lower thermal diffusivity, or larger Pr, is what breaks down the temperature. As can be seen in Figure 12, the fluid's temperature rises as the radiation parameterRd rises. In this instance, as Rd increases, the absorption coefficient falls, increasing the rate of radiative heat transfer. To examine the effect of the K_c homogeneous reaction parameter, refer to Figure 13. It is observed that there is a drop in fluid concentration with increasing K_c. The effect of the heterogeneous reaction parameter K_r on the concentration profile is depicted in Figure 14. An increase in K_r values corresponds to an increase in fluid concentration. The impact of Schmidt number Sc on the concentration profile is depicted in Figure 15. An increase in the Schmidt number led to an increase in particle concentration.The impact of Peclet number Pe on the microorganism profile is depicted in Figure 16. A direct correlation has been observed between the increased Pe and the microorganism's better density. The impact of Lewis number Le on the microorganism profile is depicted in Figure 17. Given that the mass diffusion and the Lewis number were inversely related, the concentration distribution shrank.

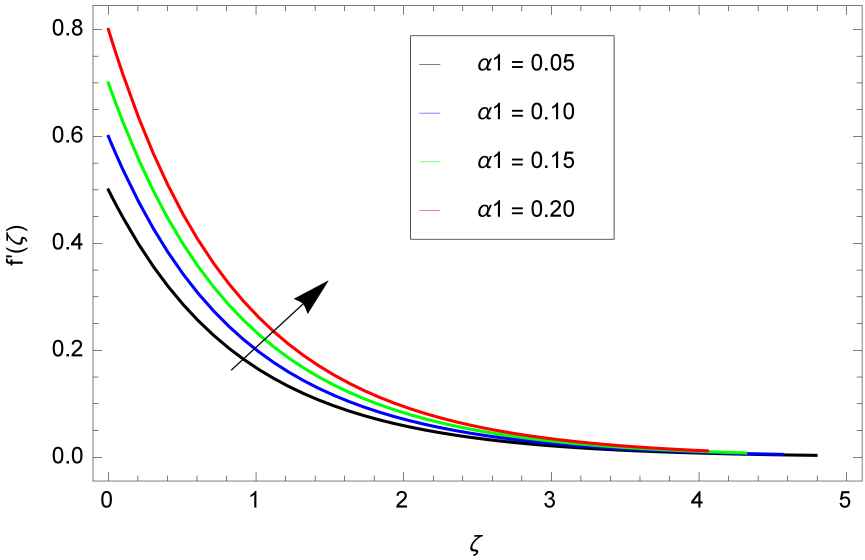

FIGURE 2. Impact of $\alpha 1$ on $f'(\zeta)$.

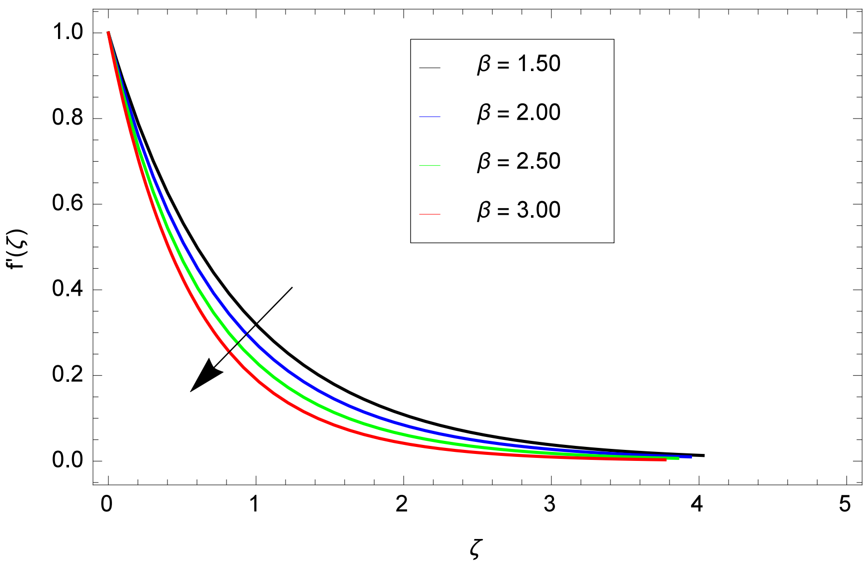

FIGURE 3. Impact of β on $f'(\zeta)$.

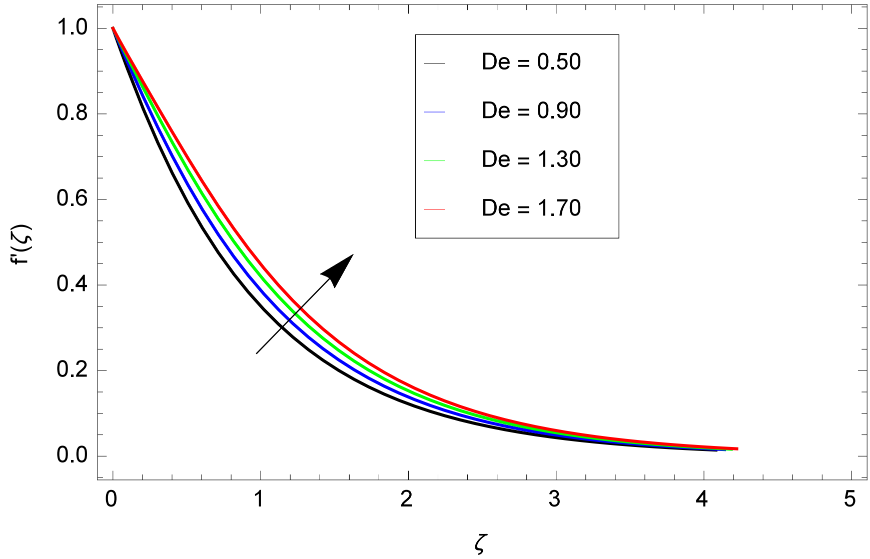

FIGURE 4. Impact of De on $f'(\zeta)$.

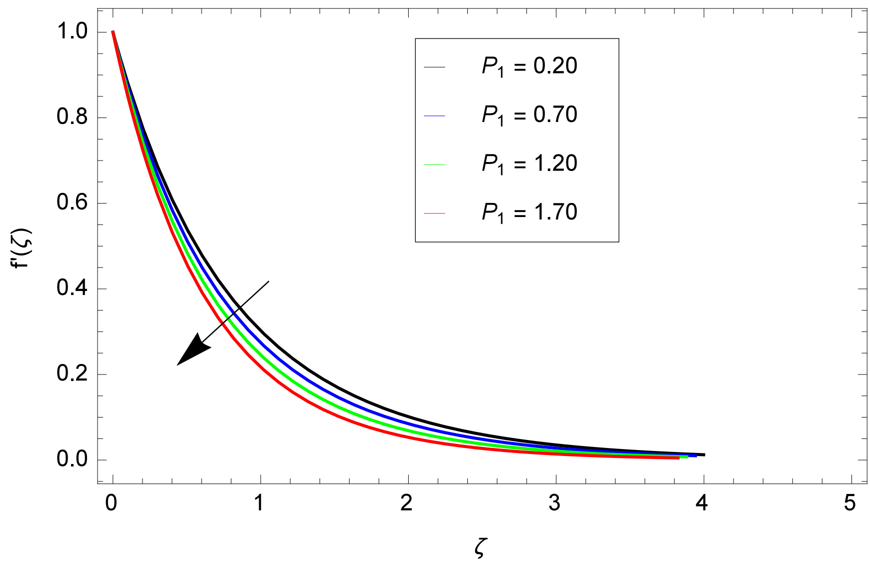

FIGURE 5. Impact of $P1$ on $f'(\zeta)$.

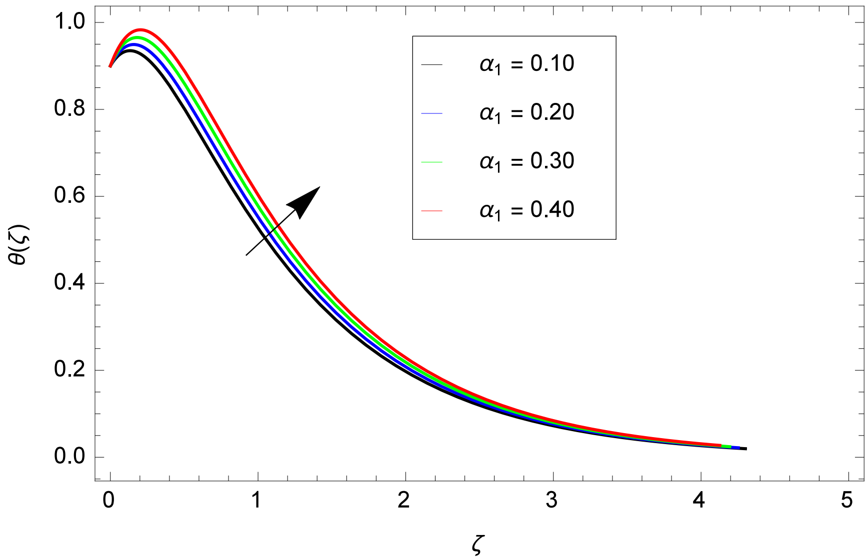

FIGURE 6. Impact of $\alpha1$ on $\theta(\zeta)$.

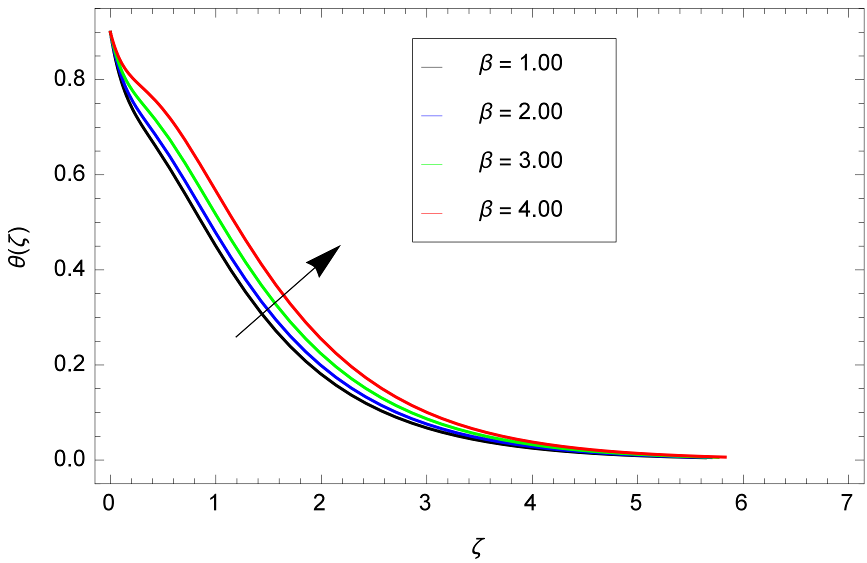

FIGURE 7. Impact of β on $\theta(\zeta)$.

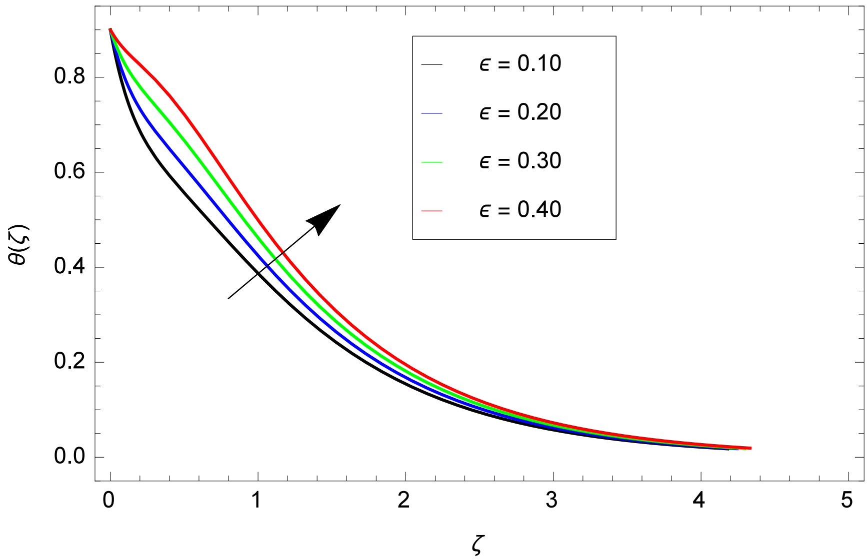

FIGURE 8. Impact of ε on $\theta(\zeta)$.

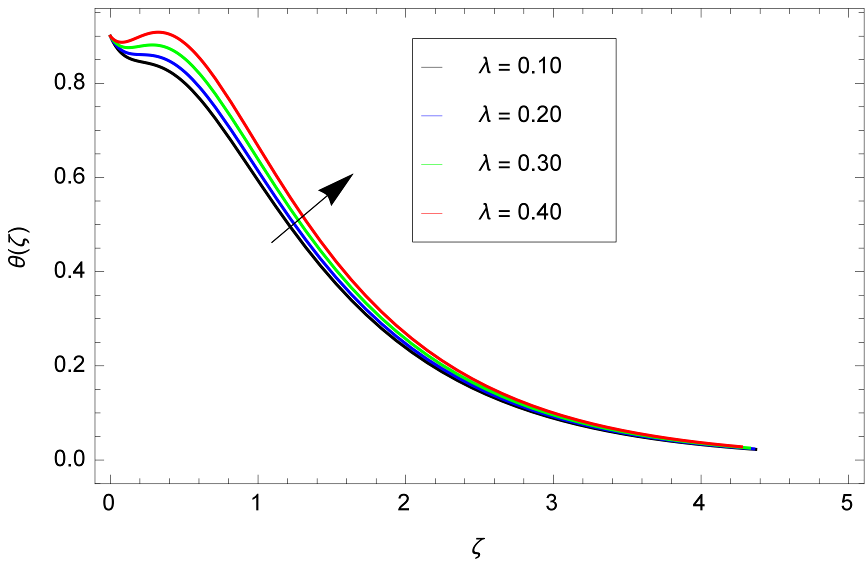

FIGURE 9. Impact of λ on $\theta(\zeta)$.

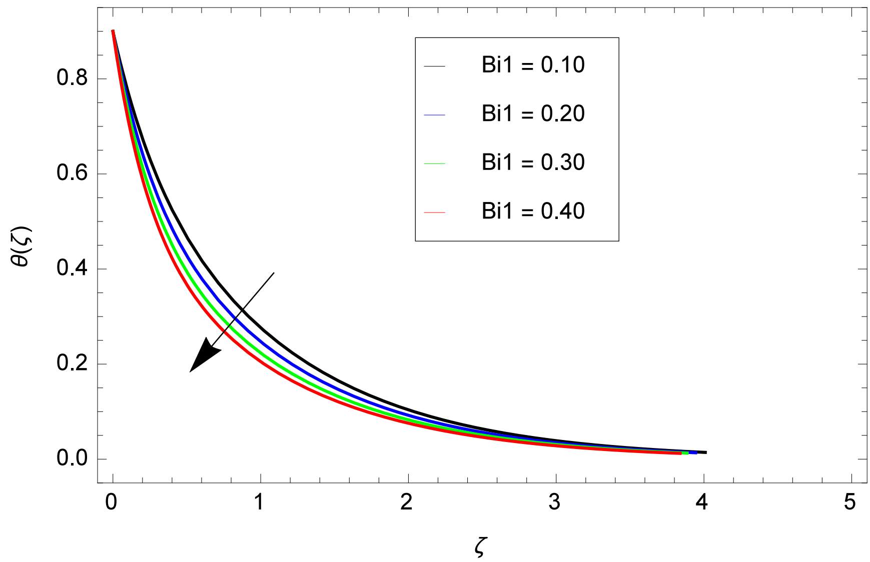

FIGURE 10. Impact of $Bi1$ on $\theta(\zeta)$.

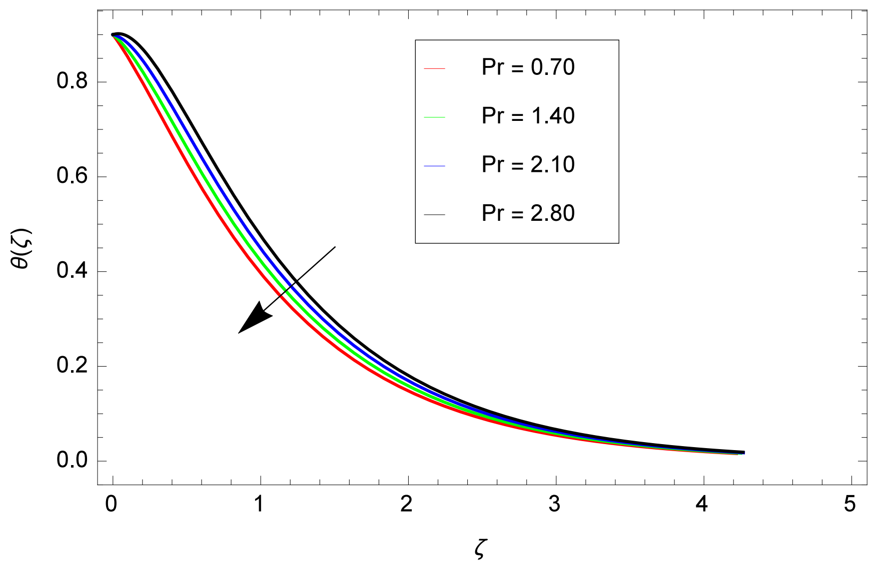

FIGURE 11. Impact of Pr on $\theta(\zeta)$.

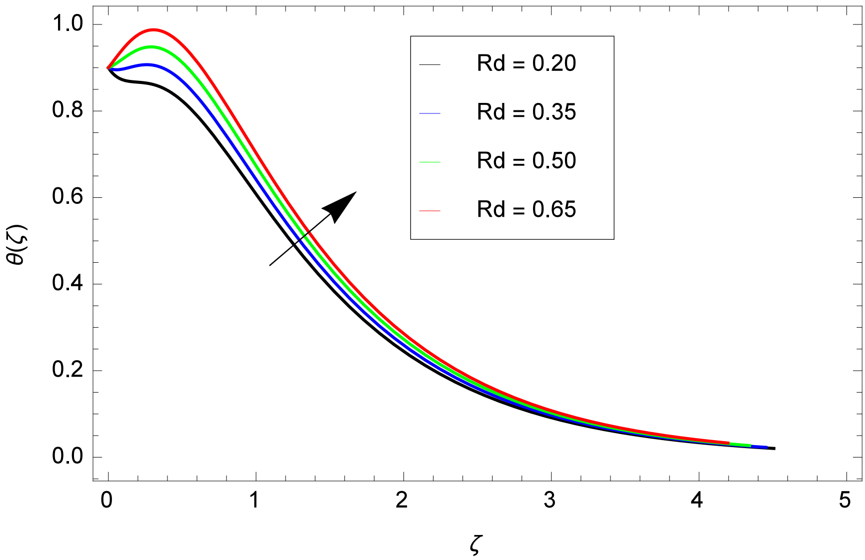

FIGURE 12. Impact of Rd on $\theta(\zeta)$.

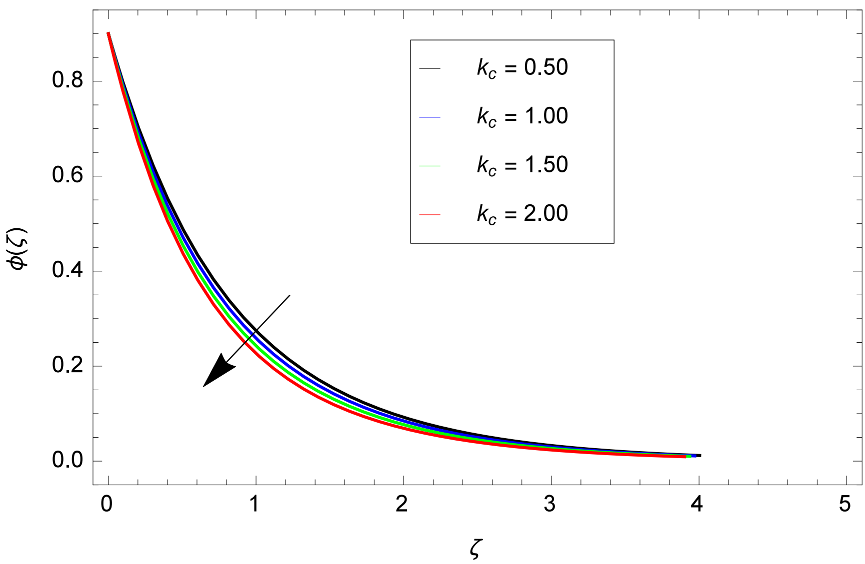

FIGURE 13. Impact of K_c on $\phi_1(\zeta)$.

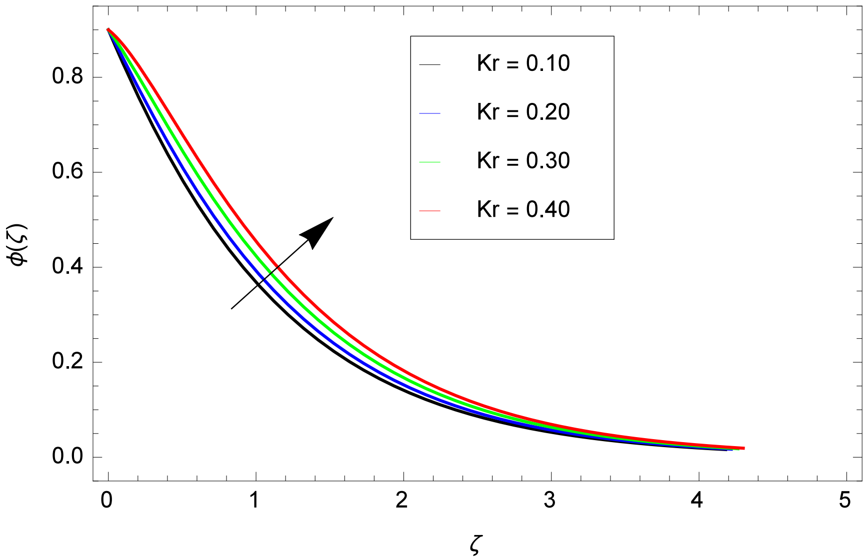

FIGURE 14. Impact of K_r on $\phi_1(\zeta)$.

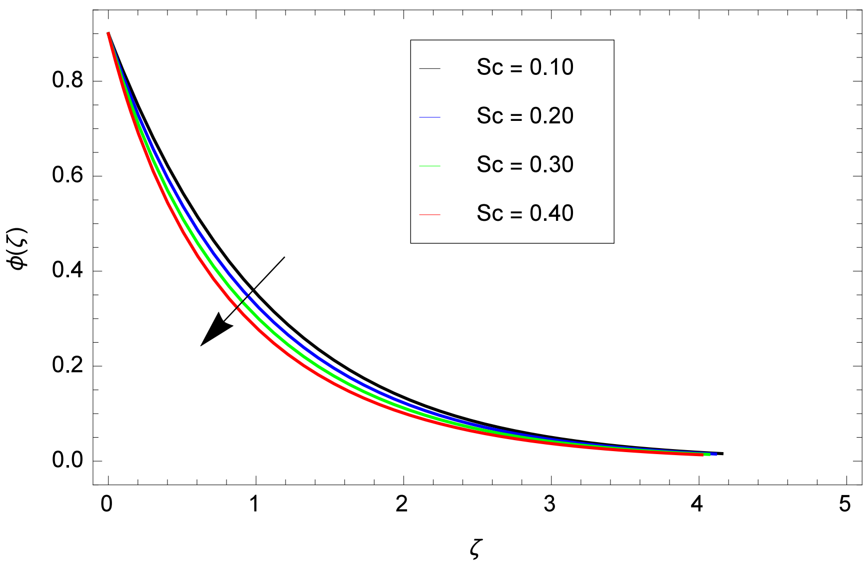

FIGURE 15. Impact of Sc on $\phi_1(\zeta)$.

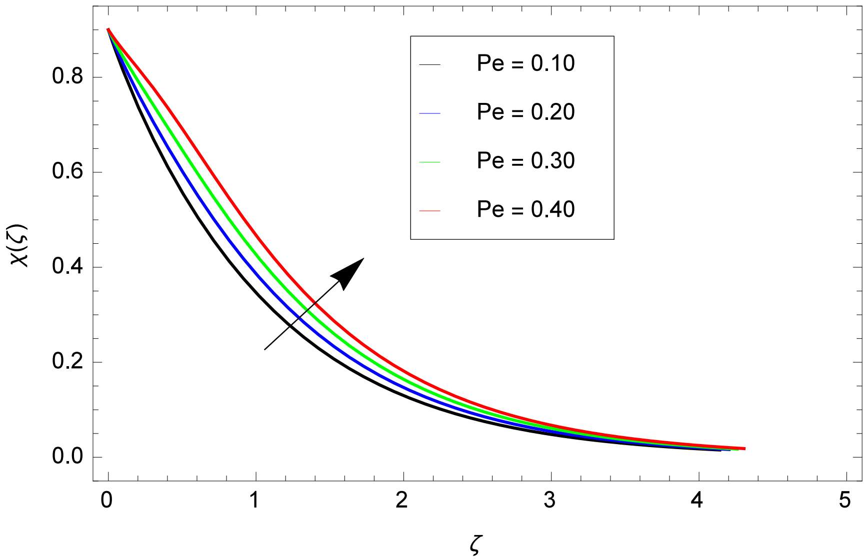

FIGURE 16. Impact of Pe on $\chi(\zeta)$.

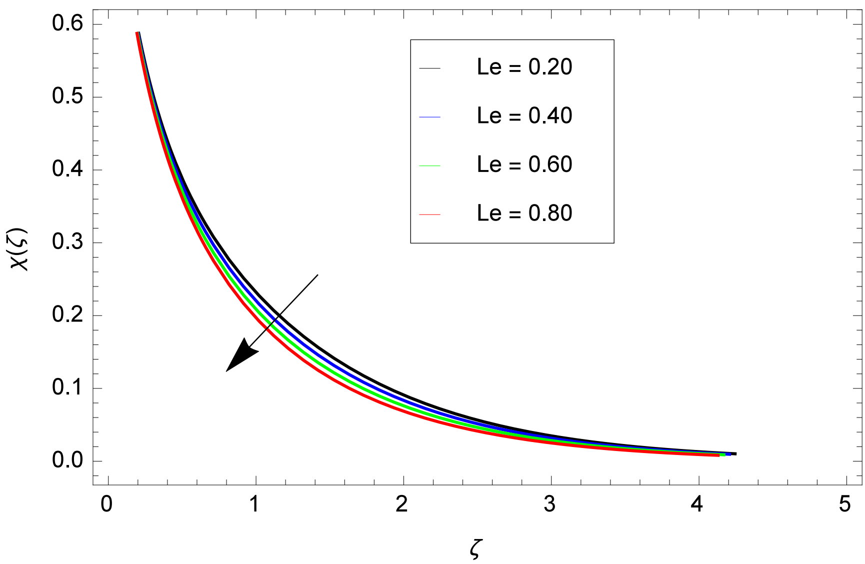

FIGURE 17. Impact of Le on $\chi(\zeta)$.

The microorganism transfer rate increases for some values of some parameters, as shown in Table 1.

Table 1. Values are computed of $-\chi'(0)$ for various values of Pe, Le, Sc.

Pe	Le	Sc	$-\chi'(0)$
0.1	0.2	0.3	0.28315
0.2			0.27328
0.3			0.37022
	0.5		0.33001
	0.7		0.32403
		0.6	0.61957
		0.9	0.85330
		1.2	1.14321

5. Conclusion

The hydromagnetic flow of Sutterby nanofluid by Darcy-Forchheimer over a curved stretched sheet with thermal radiation and the presence of magnetic dipoles was studied using a mathematical model of homogeneous heterogeneous chemical processes. Following similarity modifications, the resulting non-dimensional differential equations were obtained, and the outcomes were provided numerically. The following are the primary points:

- The velocity has increased with the curvature parameters $\alpha 1$,, De, and λ and decreased with the rising ferromagnetic parameters β and $p1$.
- The temperature rises as $\alpha 1$, β, and Rd grow and falls as Pr increases.
- Larger heterogeneous-reaction K_r and Schmidt at Sc result in a higher concentration rate, but larger homogeneous-reaction K_c represents a decrease in the concentration rate.
- The density of the micro-organism increases with Pe and decreases with Le.

Acknowledgments

This research project was supported by the management of Bayero University Kano, Nigeria.

Declarations

Conflict of Interests

The authors have no conflict of interests.

Authors contribution

A.H.U., and W.K. formulated, solved the problem, wrote the draft. A.H.U. performed the investigations. A.H.U. and W.K. sketched the graphs. A.H.U performed the supervision and provide the funding.

Statement about data

Availability exists for whole of the data.

Consent for publication

The authors agreed to publish this article in the Bangmod International Journal of Mathematical & Computational Science.

References

[1] J.L. Sutterby, Laminar converging flow of dilute polymer solutions in conical sections: Part I. Viscosity data, new viscosity model, tube flow solution, AIChE Journal 12(1) (1966) 63–68. https://doi.org/10.1002/aic.690120114.

[2] J.L. Sutterby, Laminar converging flow of dilute polymer solutions in conical sections II, Transactions of the Society of Rheology 9(2) (1965) 227–241. https://doi.org/10.1122/1.549024.

[3] R.L. Batra, M. Eissa, Helical flow of a Sutterby model fluid, Polymer-Plastics Technology and Engineering 33(4) (1994) 489–501. https://doi.org/10.1080/03602559408010743.

[4] M.M. Fayyadh, K. Naganthran, M.F. Basir, I. Hashim, R. Roslan, Radiative MHD Sutterby Nanofluid Flow Past a Moving Sheet: Scaling Group Analysis, Mathematics 8(9) (2020) 1430. https://doi.org/10.3390/math8091430.

[5] T. Hayat, S. Ayub, A. Alsaedi, A. Tanveer, B. Ahmad, Numerical simulation for peristaltic activity of Sutterby fluid with modified Darcy's law, Results in physics 7 (2017) 762–768. https://doi.org/10.1016/j.rinp.2017.01.038.

[6] N.A. Mir, M. Farooq, M. Rizwan, F. Ahmad, S. Ahmad, B. Ahmad, Analysis of thermally stratified flow of Sutterby nanofluid with zero mass flux condition, Journal of Materials Research and Technology 9(2) (2020) 1631–1639. https://doi.org/10.1016/j.jmrt.2019.11.088.

[7] P.Z. Forchheimer, Wasserbewegungdurch Boden, Zeitschrift des Vereins Deutscher Ingenieure 45 (1901) 1781–1788.

[8] D.A. Nield, A. Bejan, Convection in porous media, New York, Springer, 2006.

[9] N. Kishan, S. Maripala, Thermophoresis and viscous dissipation effects on Darcy-Forchheimer MHD mixed convection in a fluid saturated porous media, Advances in applied science Research 3 (2012) 60–74.

[10] A. Rauf, Z. Abbas, S.A. Shehzad, T. Mushtaq, Thermally Radiative Viscous Fluid Flow Over Curved Moving Surface in Darcy-Forchheimer Porous Space, Communications in Theoretical Physics 71 (2019) 259. https://doi.org/10.1088/0253-6102/71/3/259.

[11] S. Jagadha, P. Amrutha, MHD Boundary Layer Flow of Darcy-Forchheimer Mixed Convection in a Nanofluid Saturated Porous Media with Viscous Dissipation, International Journal of Applications and Applied Mathematics 4 (2019) 117–134.

[12] M.R. Eid, F. Mabood, Two-phase permeable non-Newtonian cross-nanomaterial flow with Arrhenius energy and entropy generation: Darcy-Forchheimer model, Physica Scripta 95(10) (2020) 105209. https://doi.org/10.1088/1402-4896/abb5c7.

[13] M.R. Eid, Thermal characteristics of 3D nanofluid flow over a convectively heated Riga surface in a Darcy-Forchheimer porous material with linear thermal radiation: an optimal analysis, Arabian Journal for Science and Engineering 45 (2020) 9803–9814. https://doi.org/10.1007/s13369-020-04943-3.

[14] M.R. Eid, F. Mabood, Entropy analysis of a hydromagnetic micropolar dusty carbon NTs-kerosene nanofluid with heat generation: Darcy-Forchheimer scheme, Journal of Thermal Analysis and Calorimetry 20 (2020) 1–8.
[15] H.I. Andersson, O.A. Valnes, Flow of a heated ferrofluid over a stretching sheet in the presence of a magnetic dipole, Acta Mechanica 128 (1998) 39–47. https://doi.org/10.1007/BF01463158.
[16] T. Hayat, S. Ahmad, M.I. Khan, A. Alsaedi, Exploring magnetic dipole contribution on radiative flow of ferromagnetic Williamson fluid, Results in physics 8 (2018) 545–551. https://doi.org/10.1016/j.rinp.2017.11.040.
[17] L.R. Titus, A. Abraham, Heat transfer in ferrofluid flow over a stretching sheet with radiation, International Journal of Engineering Research and Technology 3 (2014) 2198–2203.
[18] G.H. Kefayati, Natural convection of ferrofluid in a linearly heated cavity utilizing LBM, Journal of Molecular Liquids 191 (2014) 1–9. https://doi.org/10.1016/j.molliq.2013.11.021.
[19] S. Afkhami, Y. Renardy, Ferrofluids and magnetically guided superparamagnetic particles in flows: a review of simulations and modeling, Journal of Engineering Mathematics 107 (2017) 231–251. https://doi.org/10.1007/s10665-017-9931-9.
[20] W.R. Williams, M.T. Stenzel, X. Song, Schmidt LD. Bifurcation behavior in homogeneous-heterogeneous combustion: I. Experimental results over platinum, Combustion and flame 84(3–4) (1991) 277–291. https://doi.org/10.1016/0010-2180(91)90006-W.
[21] W.R. Williams, J. Zhao, L.D. Schmidt, Ignition and extinction of surface and homogeneous oxidation of NH3 and CH4, AIChE journal 37(5) (1991) 641–649. https://doi.org/10.1002/aic.690370502.
[22] J.H. Merkin, A model for isothermal homogeneous-heterogeneous reactions in boundary-layer flow, Mathematical and Computer Modelling 24(8) (1996) 125–136. https://doi.org/10.1016/0895-7177(96)00145-8.
[23] T. Hayat, A. Kiran, M. Imtiaz, A. Alsaedi, Effect of homogeneous-heterogeneous reactions in stagnation point flow of third grade fluid past a variable thickness stretching sheet, Neural Computing and Applications 30(10) (2018) 3071–3080. https://doi.org/10.1007/s00521-017-2913-z.
[24] C.S. Raju, N. Sandeep, S. Saleem, Effects of induced magnetic field and homogeneous-heterogeneous reactions on stagnation flow of a Casson fluid, Engineering Science and Technology, an International Journal 19(2) (2016) 875–887. https://doi.org/10.1016/j.jestch.2015.12.004.
[25] M.I. Khan, T. Hayat, M.I. Khan, A. Alsaedi, A modified homogeneous-heterogeneous reaction for MHD stagnation flow with viscous dissipation and Joule heating, International Journal of Heat and Mass Transfer 113 (2017) 310–317. https://doi.org/10.1016/j.ijheatmasstransfer.2017.05.082.
[26] T. Hayat, M.I. Khan, M. Farooq, T. Yasmeen, A. Alsaedi, Stagnation point flow with Cattaneo-Christov heat flux and homogeneous-heterogeneous reactions, Journal of Molecular Liquids 220 (2016) 49–55. https://doi.org/10.1016/j.molliq.2016.04.032.
[27] B.C. Sakiadis, Boundary-layer behavior on continuous solid surfaces: I. Boundary-layer equations for two-dimensional and axisymmetric flow, AICHE Journal 7(1) (1961) 26–28. https://doi.org/10.1002/aic.690070108.

[28] R. Muhammad, M.I. Khan, M. Jameel, N.B. Khan, Fully developed Darcy-Forchheimer mixed convective flow over a curved surface with activation energy and entropy generation, Computer Methods and Programs in Biomedicine 188 (2020) 105298. https://doi.org/10.1016/j.cmpb.2019.105298.

[29] S. Ahmad, S. Nadeem, N. Muhammad, Boundary layer flow over a curved surface imbedded in porous medium, Communications in Theoretical Physics 71(3) (2019) 344. https://doi.org/10.1088/0253-6102/71/3/344.

[30] W.A. Khan, M. Waqas, M. Ali, F. Sultan, M. Shahzad, M. Irfan, Mathematical analysis of thermally radiative time dependent Sisko nanofluid flow for curved surface, International Journal of Numerical Methods for Heat and Fluid Flow 9 (2019) 3498–3514.

[31] S.J. Liao, An explicit, totally analytic approximate solution for Blasius' viscous flow problems, International Journal of Non-Linear Mechanics 34 (1999) 759–778. https://doi.org/10.1016/S0020-7462(98)00056-0.

[32] S. Liao, Beyond perturbation: introduction to the homotopy analysis method, CRC press, 2003.

[33] S.J. Liao, Homotopy analysis method in nonlinear differential equations, Higher Education Press Beijing and Springer-Verlag Berlin Heidelberg, 2012.

[34] M. Ramzan, P. Kumam, W. Watthayu, Analyzing heat and mass transport phenomena using the Casson-nanofluid model in the context of Vacuum Pump Oil (VPO) and Cattaneo-Christov heat flux applications, Case Studies in Thermal Engineering 53 (2024) 103796. https://doi.org/10.1016/j.csite.2023.103796.

[35] A.H. Usman, Z. Shah, W. Khan, Semi-analytical investigation on MHD oldroyd-b nanofluid flow under stratification conditions via an exponentially stretching surface, Bangmod International Journal of Mathematical and Computational Science 8 (2022) 65–99. https://doi.org/10.58715/bangmodjmcs.2022.8.6.

[36] M. Ramzan, M. Javed, S. Rehman, A. Saeed, P. Kumam, A.M. Galal, Irreversibility analysis of melting rheology in micropolar Al2O3-mineral oil nanofluid flow with homogeneous and heterogeneous reactions, Numerical Heat Transfer, Part A: Applications 85(3) (2024) 444–466. https://doi.org/10.1080/10407782.2023.2187903.

[37] N.S. Khan, Bioconvection in second grade nanofluid flow containing nanoparticles and gyrotactic microorganisms, Brazilian Journal of Physics 48 (2018) 227–241. https://doi.org/10.1007/s13538-018-0567-7.

[38] Z. Shah, S. Islam, T. Gul, E. Bonyah, M.A. Khan, The electrical MHD and hall current impact on micropolar nanofluid flow between rotating parallel plates, Results in physics 9 (2018) 1201–1214. https://doi.org/10.1016/j.rinp.2018.01.064.

[39] S. Zuhra, N.S. Khan, M.A. Khan, S. Islam, W. Khan, E. Bonyah, Flow and heat transfer in water based liquid film fluids dispensed with graphene nanoparticles, Result Phys 8 (2018) 1143–1157. https://doi.org/10.1016/j.rinp.2018.01.032.

[40] S. Zuhra, N.S. Khan, S. Islam, Magnetohydrodynamic second-grade nanofluid flow containing nanoparticles and gyrotactic microorganisms, Computational and Applied Mathematics 37(5) (2018) 6332–6358. https://doi.org/10.1007/s40314-018-0683-6.

[41] M.A. Chaudhary, J.H. Merkin, A simple isothermal model for homogeneous-heterogeneous reactions in boundary-layer flow. I Equal diffusivities, Fluid dynamics research 16(6) (1995) 311. https://doi.org/10.1016/0169-5983(95)00015-6.